

Poly(methyl methacrylate) and silica nanocomposites as new materials for polymeric optical devices

Rafael Affonso Netto^{1*} , Fabrícia Faria de Menezes² , Rubens Maciel Filho² 
and Julio Roberto Bartoli^{1*} 

¹*Laboratório de Materiais Dielétricos, Ópticos e Nanocompósitos – LMDON, Departamento de Materiais e Bioprocessos – DEMBio, Faculdade de Engenharia Química – FEQ, Universidade Estadual de Campinas – UNICAMP, Campinas, SP, Brasil*

²*Laboratório de Otimização, Projetos e Controle Avançado – LOPCA, Departamento de Desenvolvimento de Processos e Produtos – DDPP, Faculdade de Engenharia Química – FEQ, Universidade Estadual de Campinas – UNICAMP, Campinas, SP, Brasil*

*netto.affonso@gmail.com; bartoli@unicamp.br

Abstract

PMMA is one of the most used polymers for optical applications, due to its well-known optical properties and low-cost. PMMA/fumed silica nanocomposites were synthesized by in situ polymerization under sonication to produce optical materials using two types of silica, a PDMS surface-modified and an unmodified one. Silica content and sonication amplitude effects on nanocomposites properties were studied by factorial experimental designs. Nanocomposites retained the high transparency of pristine PMMA, especially at lower levels of silica and sonication. Rheological analysis indicated better dispersion of the unmodified silica in PMMA. Dispersed silica in the PMMA nanocomposites decreased the PMMA refractive index by 0.012, making PMMA/fumed silica suitable for the cladding layer of PMMA-core waveguides, resulting in the total reflectance phenomenon for light guiding. Therefore, PMMA/fumed silica nanocomposites provide promising materials for polymer optical devices, such as optical fibers and panels, optical sensors and biosensors, photonic platforms, daylighting, and multi-touchscreen displays.

Keywords: *polymer optical fibers, in situ polymerization, fumed silica, sonication, rheology.*

How to cite: Affonso Netto, R., Menezes, F. F., Maciel Filho, R., & Bartoli, J. R. (2022). Poly(methyl methacrylate) and silica nanocomposites as new materials for polymeric optical devices. *Polímeros: Ciência e Tecnologia*, 32(3), e2022031. <https://doi.org/10.1590/0104-1428.20220009>

1. Introduction

Optical fibers and waveguides are devices that transmit light signals with high speeds and low losses^[1]. Light is continuously reflected inside a continuous core coated with a cladding, (total internal reflection)^[1,2] which has a lower refractive index by, at least, 0.002 to 0.005, depending on the diameter of the core (usually 10 μm in monomode and 50 μm in multimode fibers)^[1]. This difference between refractive indexes may be gradual or stepwise and the materials used for core and cladding may be silica or polymer-based^[1]. Silica optical fibers (SOF) show the best optical properties, despite their low elastic limit hindering flexibility unless the fiber is produced with reduced diameters (less than 125 μm)^[1,2], which might save space and weight, but causes handling problems, especially at connections, raising costs^[1]. SOFs were revolutionary at optoelectronics, photonics and telecommunications, enabling high-speed data transfer (higher than 10 Gb/s) free of electromagnetic interferences^[1,2].

Alternatively, polymeric optical fibers (POFs) have their core and cladding made of polymers^[1-3], and the most used for POFs are poly(methyl methacrylate)

(PMMA)^[1,4], polystyrene (PS)^[5], polycarbonate (PC)^[6], cyclic olefin polymers^[7], fluorinated polymers blends, such as poly(vinylidene fluoride) (PVDF)^[8] and plasma fluorinated-surface polymers^[4]. POFs show advantages compared to silica fibers, such as flexibility, enabling manipulation like bending with small radius without transmittance losses^[1,2,9]. Assembly of POFs is easier and application of visible light (usually at 680 nm) allows detection by eye^[1]. POFs show good weathering resistance, enabling outdoor, underground, and even underwater applications^[1,2,9].

However, POFs show disadvantages compared to SOFs, such as attenuation of the transmitted signal level and bandwidth over long distances, limiting their use to a 1 km radius^[1]. Nevertheless, most of the Local Area Networks (LAN), Fiber to the Home (FTTH) technologies and industrial automation networks are located within this radius, making POFs advantageous over metallic conductors, such as copper wirings when regarding signal transmittance ratio and electromagnetic interferences^[1,9,10].

Application of polymers on optical fibers and waveguides have been widely studied due to their molecular structure

versatility in establishing different refractive indexes, their well-known transformation processes, significant cost-benefit ratio and raised flexibility limits, aspects that lead to several applications for POFs or waveguides, such as optical sensors, actuators, integrated optics, optical amplifiers, optoelectronic devices, photonic platforms, and others, industrial, automotive, aeronautics, and automation^[1,4,10].

Microstructured optical fibers (MOFs), or photonic crystals, led to a great development in fiber technology^[9,10], exhibiting different properties compared with regular fibers since a MOF structure consists of a geometric arrangement of repeating microscopic cavities along the cross-section of the fiber, considerably reducing the optical losses^[11,12]. Recently, Cordeiro et al.^[7] assembled a low-cost, laboratory bench extrusion machine to manufacture polymeric MOFs in a single-step process. In another work^[13], nanocomposite films made from PMMA and fumed silica produced by sonication enabled promising applications as solid-state electrolytes for electrochromic windows and optoelectronic devices.

From another perspective, nanotechnology enables advances in the development of new, high-performance, innovative nanocomposite materials^[14-27], with unique properties deriving from a synergistic relationship between a polymer matrix and a nanometric filler^[25-27] that depends on particles dimensions, chemical affinity between polymer and particles and their dispersion on a nanometric scale within the matrix^[25-27]. New properties of nanocomposites, such as mechanical and thermal enhancements, electric conductivity and different chemical reactivity depend on the type of filler, and might not be observed with micrometric or macrometric particles^[28-39]. Several studies on PMMA nanocomposites showed that their mechanical properties can be enhanced without impairing their remarkable optical properties^[12,13,34]. Reinforcement resulted by adding silica nanoparticles to amorphous polymers stems mainly from molecular stiffening of polymer chains due to interactions with nanoparticles, which show larger surface area interacting with these chains, increasing their physical adsorption^[40-45]. Light's wavelength is higher than particles nanometric size, therefore, these particles would not influence the optical properties of the nanocomposites^[46]. Polar OH groups on silica particles also interact with the dipoles on PMMA pendant groups through Van der Waals interactions. Silica particles have been widely studied in composite materials, showing versatile properties and enabling materials for various applications^[43,44,47,48].

Several methods were applied to achieve homogeneous particle dispersion in nanocomposites, avoiding particle agglomerates or clusters^[44,45]. One of these methods, in situ polymerization, consists in placing the filler inside the reaction site from the beginning of the reactions^[44,45]. Another method, sonication with an ultrasound probe, also provides advantages, such as lower reaction temperatures, higher filler particles or additives dispersion achieved on the reaction site by cavitation, breaking of particle clusters or agglomerates, facilitated mass transfer phenomenon, and elevated reaction conversions. Adequate sonication energy, time, and amplitude enables better control over polymer molar mass and morphology^[49-51].

PMMA nanocomposites, with adequate cost-benefit ratio, are promising materials for optical devices such as optical fibers, waveguides and optical substrates for touch screens. In this study, PMMA and fumed silica nanocomposites were synthesized by in situ polymerization, in chloroform solution under sonication with ultrasound probe. Chloroform was chosen because it has the same solubility parameter as PMMA (19 MPa^{0.5}), dissolving both PMMA and the MMA monomer, allowing better heat dissipation, maintaining a low viscosity of the reaction medium and favoring intercalation of silica nanoparticles with the growing polymeric chains. In addition, polymerization temperature is lower using chloroform (60°C). Rapid volatilization of chloroform is also useful in the preparation of PMMA films by casting.

Objectives of this work were to obtain PMMA nanocomposites applicable on optical devices. Two types of commercial fumed silica nanoparticles were used as fillers, one is surface-modified with polydimethylsiloxane (PDMS) and the other is unmodified. Optical and rheological properties were analyzed using two experimental designs as a function of nanoparticles content (2% to 6%, in weight) and ultrasound relative amplitude (26% to 50%). Range of nanosilica amount used in this work was assumed from Abramoff and Covino^[38]. According to the authors, transmittance of PMMA, filled with fumed silica, decreases with increasing filler content, but increases as nanofiller dispersion improves within the matrix, which occurs as particles specific surface increases; that is, decrease in primary particle size.

Several factors that can influence the course of an ultrasound-assisted polymerization, such as intensity of the ultrasound amplitude, since the amount of bubbles generated in the reaction medium is closely linked to this variable, and affects the intensity of the cavitation phenomenon. Therefore, applied ultrasound amplitude is a factor that must be studied and planned if used in a polymerization. Price et al.^[40,41] studied ultrasound-assisted polymerization of methyl methacrylate (MMA) and its degradation, with an effect on the molar mass of the obtained polymer. Degradation of PMMA molar mass occurs with increasing sonication time, inversely proportional to the square root of the ultrasound intensity.

2. Materials and Methods

2.1 Materials

MMA (99.9%) was supplied by UNIGEL. Silica nanoparticles were: AEROSIL® 300 (99.8%), average primary particle size of 7 nm, supplied by EVONIK, named *nanosilica-A*; and CAB-O-SIL® TS720 (99.4%), surface-modified with polydimethylsiloxane (PDMS), average particle size around 0.4 µm, supplied by CABOT®, named *nanosilica-C*. Chloroform (99.8%) was used as solvent, supplied by Synth. AIBN (2,2'-azobis-(isobutyronitrile)) was used as initiator, supplied by DuPont. Gaseous N₂ (99.996%) was supplied by White Martins.

2.2 Synthesis of nanocomposites

Nanocomposites were synthesized by in situ, solution, chain-growth polymerization with sonication, gaseous N₂ as

inert atmosphere, and named according to the type of silica nanoparticles used. Chloroform (75 mL) was added to each amber flask (125 mL). Next, silica nanoparticles were added following the experimental designs (Table 1), with triplicate central points ($2^2 + 1$). Next, 25 mL of MMA and 0.1927 g of AIBN were added, in a mole ratio of 200 MMA : 1 AIBN. Proportion between MMA and chloroform was chosen to ensure constant solution viscosity and proper heat dissipation throughout the reactions. Seven nanocomposites samples were synthesized for each nanosilica type. An unfilled PMMA sample was also produced without silica, named pristine, totaling 15 samples.

Polymerizations started with sonication (Q700 processor, QSONICA®, 700 W, 20 kHz) applied with a probe (diameter: 6.4 mm, maximum amplitude: 170 μm) in pulses of 1 s for 25 min of active sonication at the beginning of the reaction (50 min total), for all samples under inert N_2 atmosphere flow (5.0 L/min). Relative amplitude of sonication probe ranged from 26% to 50% (Table 1). Next, the flasks were closed, sealed and kept in an oven at 60°C for 24 h to complete polymerization. Afterwards, samples solutions were used to produce films by casting. Precipitation of the synthesized samples was also conducted in methanol (12 hours, in ice bath), followed by filtration and drying in an oven, at 70°C for 72 h. Precipitated nanocomposites and pristine PMMA samples were used to produce discs through press molding.

2.3 Preparation of nanocomposites films and discs samples

Sample films of the nanocomposites and pristine PMMA were prepared from the produced solutions by casting and left for 24 hours at room temperature at a laboratory fume hood for solvent evaporation. After drying, the films easily detached from the aluminum sheet substrate. Disc-shaped test specimens (25 mm diameter and 1 mm thick) of the nanocomposites and pristine PMMA were prepared by compression molding (155°C, 10 min).

2.4 Characterization methods

UV-visible spectroscopy analyses were performed on the nanocomposites and pristine PMMA films using a Shimadzu UV-1800 UV-Vis Spectrophotometer, wavelength range from 200 to 800 nm. Refractive index measurements were performed on the nanocomposites and pristine PMMA discs using a Carl Zeiss Abbe refractometer, at 589 nm wavelength (sodium D line light), at 23°C, with mono-bromonaphthalene

as contact liquid. Small Amplitude Oscillatory Shear (SAOS) parallel-plate rotational rheometry analyses were performed on the nanocomposites and pristine PMMA discs using a Thermo Scientific RheoStress 600 rheometer, at 190°C, under inert atmosphere (N_2), frequency range from 1.5×10^{-3} Hz (9.42×10^{-3} rad/s) to 15 Hz (94.2 rad/s), and 500 Pa stress at the linear viscoelastic regime.

3. Results and Discussions

3.1 Optical properties of the nanocomposites and pristine PMMA

3.1.1 UV-Vis transmittance

Figure 1 shows the maximum measured UV-visible transmittance for pristine PMMA as 87.4% at 600 nm wavelength, slightly lower than the 92% reference value for PMMA at 600 nm in other works^[23,24,41-43], which is associated to heterogeneities due to the casting process and possible solvent or monomer residues^[45,46]. On the other hand, the maximum transmittances on visible light for the nanocomposites films were close to pristine PMMA films. At 600 nm wavelength, transmittances were between 83.7% and 86.4% for the PMMA/nanosilica-A nanocomposites and between 82.7% and 86.1% for the PMMA/nanosilica-C nanocomposites.

The obtained values enable usage of these materials in optical devices. It should be noted that the lowest intrinsic losses by light absorption in PMMA, due to the harmonics of molecular vibrational absorption in C–H bonds, appear at 506 nm, 568 nm, and 650 nm^[38,40-47], hence, wavelengths

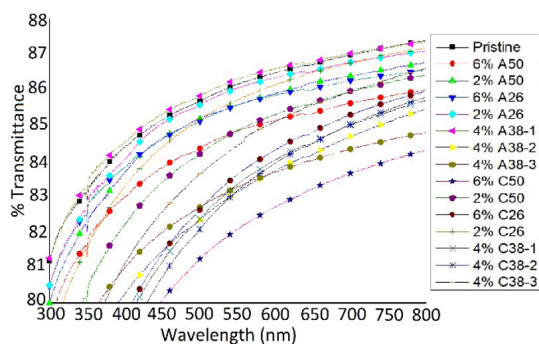


Figure 1. Transmittance values for nanocomposites and pristine PMMA films for wavelengths from 300 to 800 nm.

Table 1. Experimental design of PMMA/nanosilica-A and PMMA/nanosilica-C nanocomposites.

Samples description		Variable levels		Coded values	
PMMA/nanosilica-A	PMMA/nanosilica-C	X1: silica content (%)	X2: sonication amplitude (%)	X1	X2
2% A26	2% C26	2%	26%	-1	-1
6% A26	6% C26	6%	26%	1	-1
2% A50	2% C50	2%	50%	-1	1
6% A50	6% C50	6%	50%	1	1
4% A38-1	4% C38-1	4%	38%	0	0
4% A38-2	4% C38-2	4%	38%	0	0
4% A38-3	4% C38-3	4%	38%	0	0
Pristine PMMA		0%	38%	-	-

in the visible region are preferred for signal transmissions in PMMA core fibers^[1,38,47-49]. UV-Visible transmittances on 300, 350, 450, and 600 nm were statistically assessed for all produced nanocomposites. ANOVA (90%, $\alpha = 0.10$, Table S1 of the Supplementary Material, calculated with *Protimiza*[®]) indicated no significant differences between measured transmittances for both variables. Interactions between variables were also not significant. Figure S1 in the Supplementary Material shows the complete UV-Vis transmittance curves.

Abramoff and Covino^[38] described that the transmittance of PMMA/silica composites increases as filler dispersion improves within the polymer matrix when particles specific surface increases. Their results showed higher transmittance values for PMMA composites with nanometric particles due to their diameters being lower than light's wavelength, as described by the Rayleigh theory^[38,47]. From their results, transparency increased from 35% to 40% on PMMA/4% nanosilica films produced by in situ polymerization, at 600 nm wavelength, when particles diameter decreased from 27 nm to 7 nm. Li et al.^[13] also prepared transparent thin films of PMMA/fumed silica nanocomposites and evaluated that UV-visible transmittances of their samples increased when particles dispersion increased through the action of a surfactant. Those results are also shown on the transmittances obtained in this work, clearly showing that in situ polymerization aided by sonication yields higher filler dispersion levels in polymer matrices than other processes, but without need for additives. Nanocomposites with *Nanosilica-A* show higher transmittances than those with *Nanosilica-C*, specially at lower silica levels and higher amplitudes, indicating that these samples show the most adequate particles dispersion.

3.1.2 Refractive index

The measured refractive indexes (n) of the prepared nanocomposites were lower than the refractive index of pristine PMMA, as expected due to silica's lower index (1.4585, at 589 nm) compared to unfilled PMMA (1.4960, at 589 nm)^[23,24]. The refractive index of a suspension varies linearly with the volume fraction of dispersed particles^[47-50]. ANOVA (90%, $\alpha = 0.10$, Table S2 of the Supplementary Material) of the indexes for silica content and sonication amplitude variables showed no significant effects for the nanocomposites with *nanosilica-A* on both variables – just a slight effect ($p = 0.05$) for the silica content and amplitude interactions, whereas, for the nanocomposites with *nanosilica-C*, sonication amplitude had no significant effect but silica content ($p = 3.10^{-4}$) and interaction between the variables ($p = 0.01$) did.

For PMMA/*nanosilica-A* and PMMA/*nanosilica-C* nanocomposites the lower measured indexes (Table 2) are adequate for cladding applications due to the $\Delta n \sim 0.006$ and $\Delta n \sim 0.012$ when compared with pristine PMMA refraction index, respectively, which is enough for optical applications since it is higher than the required $\Delta n \sim 0.002$. The statistical significance observed in PMMA/*nanosilica-C* nanocomposites indexes is probably due to the effect of PDMS on the silica nanoparticle dispersion.

Results for 4% A38-3 are not available due to sample shortage. The particles or aggregates used as fillers should

Table 2. PMMA/nanosilica nanocomposites and pristine PMMA refractive indexes measured at 589 nm.

Sample	Refractive index	Sample	Refractive index
2% A26	1.4902	2% C26	1.4925
6% A26	1.4918	6% C26	1.4840
2% A50	1.4930	2% C50	1.4910
6% A50	1.4905	6% C50	1.4869
4% A38-1	1.4919	4% C38-1	1.4881
4% A38-2	1.4926	4% C38-2	1.4880
4% A38-3	-	4% C38-3	1.4879
Pristine PMMA refractive index: 1.4960			

have dimensions lower than 10% of the wavelength of incident light (589 nm) to avoid losses due to scattering by the particles (Rayleigh scattering)^[38,47-50], where shock section (Cs) of a particle depends on its diameter (d), light wavelength (λ), and relation between the refractive indices of particle and matrix (m), according to Equation 1^[50]:

$$C_s = \frac{2\pi^5 d^6}{3\lambda^4} \left(\frac{m^2 - 1}{m^2 + 1} \right)^2 \quad (1)$$

Therefore, since matching the refractive indexes of particles and matrix is impossible, reduction of losses due to light scattering in composites depends on their phase domains being smaller than light wavelength^[46-50]. The lower the Δn between particles and matrix refractive indexes, the less significant is the scattering effect^[38,46-50]. Obtained results for transmittance levels and refractive indexes are promising because Δn is high enough for the total internal reflection to happen, but is low enough to achieve low scattering levels, representing original contribution to the knowledge of technological applications for nanocomposites. In situ polymerization aided by sonication enabled the nanocomposites produced in this work to achieve higher levels of transparency and adequate refractive indexes for applications in optical devices and photonic platforms, also, Δn is directly related to particle dispersion in a polymer matrix^[38], and a slight tendency of lower Δn for the PMMA/*nanosilica-A* nanocomposites could be noted, which implies that these nanocomposites achieved higher particle dispersion levels^[38].

The numerical aperture (NA) is a critical quality that represents the light incidence angle on optical devices and depends on the difference between the refractive indexes of the materials in which devices are built^[1]. It is calculated using Equation 2^[1]:

$$NA = \left[(n_{core})^2 - (n_{cladding})^2 \right]^{\frac{1}{2}} \quad (2)$$

In polymeric waveguides, changes between 0.002 and 0.005 in the refractive index, between its core and cladding, are enough to enable total internal reflection and let light be guided through^[1-3,5]. That Δn range results in numerical apertures between 0.08 and 0.12. In this study, the numerical apertures ranged between 0.10 and 0.19 for the two types

of nanocomposites related to pristine PMMA, as estimated with the obtained refractive indexes shown in Table 2. Thus, the two types of nanocomposites synthesized in this work are promising optical materials as cladding of polymeric optical fibers with a PMMA core.

3.3 Rheological analysis

Rheological behaviors of PMMA/nanosilica nanocomposites and pristine PMMA were assessed by SAOS, parallel-plates rheometry, in molten-state. Zhao et al.^[51] demonstrated that SAOS rheometry is appropriate to determine dispersion levels of nanoparticles in polymeric nanocomposites, since rheological properties are sensitive to structural changes on a nanometric scale^[51,52]. Measuring parameters such as shear-thinning exponent (n_ω), elastic plateau at low frequencies (ω), viscosity (η), shear storage (G'), and loss (G'') moduli, contributes to assessing dispersion and determining the percolation threshold of polymeric nanocomposites that follow the power-law relationship between η and ω , as seen on Equation 3^[52]:

$$\eta = k \omega^{n_\omega} \quad (3)$$

Table 3 shows the results of the rheological analyses of the two types of nanocomposites and the pristine PMMA. Figures S3–S17 on the Supplementary Material show the rheological curves of G' , G'' , and complex viscosity (η^*), as a function of ω , for the nanocomposites and pristine PMMA. A strain sweep analysis was performed prior to the others, as seen on Figure S2 on the Supplementary Material.

Rheological analyses of the two types of nanocomposites showed increases in G' , G'' , and η^* values in the low-frequency zone ($\omega = 1.5 \times 10^{-3}$ Hz) compared to pristine PMMA, except for 6% A26, which probably had inadequate filler dispersion due to high nanosilica content (6%) and low sonication amplitude (26%). These results relate to the molecular stiffening caused in the PMMA chains by the presence of nanoparticles that restricts their relaxation^[24,40].

PMMA/nanosilica-A nanocomposites showed the highest G' values, between 0.69 to 1.56 kPa, at 2% and 4% silica contents and 38% and 50% sonication amplitudes. For 2% concentration and 50% sonication amplitude, for example, the G' modulus values were ~ 1.0 kPa and ~ 0.6 kPa for the PMMA/nanosilica-A and PMMA/nanosilica-C nanocomposites, respectively. Possibly, the nanosilica-C surface modification with PDMS lowered chemical affinity between nanoparticles and PMMA matrix, along with some plasticizing effect.

The 4% A38-2 sample shows outlier results for G' , G'' , and η^* , superior to the other central points, probably due to random errors in the preparation of this sample and/or in its rheological evaluation. In turn, ANOVA (90% confidence interval) of the G' , G'' , and η^* properties of the PMMA/nanosilica-C nanocomposites showed a significant interaction between the variables nanosilica-C content and the ultrasound amplitude level. These variables showed no significant interaction for PMMA/nanosilica-A nanocomposites, probably indicating a better dispersion of nanosilica-A in the PMMA matrix.

However, for all nanocomposites, no rheological percolation thresholds were observed, which is characterized by a plateau on the G' curve in frequencies between 10^{-2} and 10^{-3} Hz (Figures S3-S17 on Supplementary Material), meaning that rheological behavior did not change from viscoelastic to pseudo-solid, which is generally observed for polymeric nanocomposites with lamellar nanoparticles^[40,51-53]. Slopes of rheological curves (α) showed values between 1.0 and 1.4 for $G'(\omega)$ and between 0.7 and 1.0 for $G''(\omega)$, for low-frequencies. Similar results were found for pristine PMMA, $G'(\omega) = 1.25$ and $G''(\omega) = 0.8$. Linear polymers that follow the power law have typical values of $\alpha G' \sim 2$ and $\alpha G'' \sim 1$ in that region^[40]. One could attribute the values found for pristine PMMA, especially for $G'(\omega)$, to matrix effects, like molar mass and its distribution.

Kotsilkova and Pissis^[53] studied polymeric nanocomposites with reduced particle sizes (around 10 nm) properly dispersed

Table 3. Storage modulus (G'), loss modulus (G''), complex viscosity (η^*), shear thinning exponent ($-n_\omega$), storage modulus declivity ($\alpha G'$) and loss modulus declivity ($\alpha G''$) values for the nanocomposites and pristine PMMA, at the 1.5×10^{-3} Hz frequency (terminal zone).

Sample	G' (kPa)	G'' (kPa)	η^* (kPa.s)	$-n_\omega$	$\alpha G'$	$\alpha G''$
PMMA/nanosilica-A	-	-	-	-	-	-
2% A26	0.43	2.17	221.50	0.11	1.25	0.87
6% A26	0.19	0.73	75.01	0.05	0.95	0.95
2% A50	0.93	3.67	379.10	0.02	1.31	0.94
6% A50	0.32	2.17	219.60	0.05	1.39	0.92
4% A38-1	0.69	3.02	309.40	0.23	1.10	0.74
4% A38-2	1.56	6.32	650.60	0.13	1.27	0.82
4% A38-3	0.96	3.65	377.70	0.27	1.06	0.69
Pristine PMMA	0.27	1.60	162.60	0.18	1.25	0.79
PMMA/nanosilica-C	-	-	-	-	-	-
2% C26	0.38	1.56	160.80	0.11	1.10	0.87
6% C26	0.54	2.89	294.20	0.09	1.27	0.88
2% C50	0.58	3.06	311.60	0.09	1.31	0.88
6% C50	0.40	1.54	159.90	0.04	1.13	0.94
4% C38-1	0.52	2.27	233.10	0.16	1.12	0.81
4% C38-2	0.46	2.01	206.30	0.15	1.11	0.82
4% C38-3	0.38	1.80	184.50	0.08	1.28	0.89

in a matrix, and found no evidence of the characteristic plateau of the pseudo-solid behavior in G' and G'' . This is due to the change in the mechanism by which the fillers reinforce the matrix when their dimensions drop from micrometric, where reinforcement occurs due to the volume occupied by the particles between the polymer chains, to nanometric dimensions, where reinforcement occurs due to molecular stiffening caused by interactions between chains and particles^[24,40,51,53]. Thus, although the characteristic plateau was not observed, there is evidence of adequate dispersion of nanoparticles, as the G' and G'' moduli values increased in the two types of nanocomposites, compared with pristine PMMA.

Furthermore, G' and G'' values obtained for the nanocomposites prepared by in situ polymerization with sonication were about two magnitude orders higher than those reported for similar nanocomposites prepared by melt intercalation and polymer solution methods, showing the efficiency of this synthesis method in dispersing nanofillers within the polymer matrix^[40,51,52]. The outlier G' , G'' , η^* , and $-n_o$ results for 4% A38-2 appears to be due to defects located on the specimen disc caused by random factors on the compression molding process.

Relaxation time (λ) was also evaluated, calculated by the inverse of the frequency at the crossover point of the G' and G'' curves (Table S3 on the Supplementary Material) and indicates interactions between polymer and fillers since it takes longer for polymer chains to relax when exposed to oscillatory regimen, showing higher molecular stiffness^[52]. Relaxation times of PMMA/nanosilica-A were relatively longer than those of PMMA/nanosilica-C nanocomposites and, in general, both were longer than pristine PMMA. Nanosilica-A seems more adequately dispersed in the PMMA matrix, inferred by the longer chain relaxation times, compared with the modified silica. On the other hand, the lowest values for relaxation times were found for the highest levels of silica (6% wt.), modified or not, which were, in general, even lower than those of pristine PMMA. Therefore, rheological results for both types of PMMA/nanosilica nanocomposites: G' , G'' , η^* , n_o , and λ , contributed to the characterization of silica dispersion in the polymeric matrix. As noted, unmodified silica showed results significantly superior to those of surface-modified silica, especially in the experimental designs with lower and intermediate silica content.

4. Conclusions

A simple route was proposed for synthesis of PMMA/nanosilica optical nanocomposites by in situ solution polymerization under sonication. Optical and rheological properties of the nanocomposites were studied using experimental designs to assess the effects of the variables: nanosilica content (2% to 6% wt) and relative amplitude of sonication (26% to 50%). Synthesis method was effective in producing PMMA/silica nanocomposites with very adequate nanoparticles dispersion, as indicated by improved rheological results, storage and loss moduli, and complex viscosity, especially at lower levels of nanosilica, which also maintained the high UV-visible transmittance of PMMA. Also, the reduced refractive indexes of nanocomposites

compared with PMMA make them suitable materials for cladding of optical fibers or waveguides. Therefore, this work provides an interesting approach to the production of optical nanocomposites based on PMMA, enabling usage of these materials for applications in optical devices, such as polymeric optical fibers, waveguides, sensors and optical substrates for touch screens, showing the potential of the properties of composite materials.

5. Author's Contribution

Conceptualization – Julio Roberto Bartoli.

Data curation – Rafael Affonso Netto; Julio Roberto Bartoli.

Formal analysis – Rafael Affonso Netto; Julio Roberto Bartoli.

Funding acquisition – Julio Roberto Bartoli.

Investigation – Rafael Affonso Netto; Fabrícia Farias de Menezes.

Methodology – Rafael Affonso Netto.

Project administration – Julio Roberto Bartoli.

Resources – Julio Roberto Bartoli.

Software – NA.

Supervision – Julio Roberto Bartoli; Rubens Maciel Filho.

Validation – Julio Roberto Bartoli.

Visualization – Julio Roberto Bartoli; Rafael Affonso Netto.

Writing – original draft – Rafael Affonso Netto.

Writing – review & editing – Julio Roberto Bartoli.

6. Acknowledgements

The authors acknowledge: “Conselho Nacional de Desenvolvimento Científico e Tecnológico” – CNPq, for the financial support – Grant Number 131785/2016-8. Dr. M. I. R. B. Schiavon (FEQ/UNICAMP), A. C. da Costa (IFGW/UNICAMP), Dr. M. H. Ara and I. S. Tertuliano (LFS/EPUSP), Prof. Edson N. Ito (DEMat/UFRN) for the supplied nanoparticles and provided characterizations, UNIGEL® and DuPont™ for the supplied chemicals, and Espaço da Escrita – Pró-Reitoria de Pesquisa – UNICAMP, for the provided language services.

7. References

- Ishigure, T., Horibe, A., Nihei, E., & Koike, Y. (1995). High-bandwidth, high-numerical aperture graded-index polymer optical fiber. *Journal of Lightwave Technology*, 13(8), 1686-1691. <http://dx.doi.org/10.1109/50.405310>.
- Bartoli, J. R. (2000). *Development and characterization of graded-index polymeric films for optical guides and sensors*. In *14th International Conference on Optical Fiber Sensors* (pp. 838-841). Bellingham: Society of Photo-Optical Instrumentation Engineers.
- Peng, G.-D., Ji, P. N., & Wang, T. (2004). *Development of special polymer optical fibers and devices*. In: *Proceedings of SPIE 5595: Active and Passive Optical Components for WDM Communications IV* (pp. 138-152) Bellingham: Society of Photo-Optical Instrumentation Engineers.

4. Giacón, V. M., Padilha, G. S., & Bartoli, J. R. (2015). Fabrication and characterization of polymeric optical by plasma fluorination process. *Optik*, 126(1), 74-76. <http://dx.doi.org/10.1016/j.ijleo.2014.08.152>.
5. Kaino, T., Fujiki, M., & Nara, S. (1981). Low-loss polystyrene core-optical fibers. *Journal of Applied Physics*, 52(12), 7061-7063. <http://dx.doi.org/10.1063/1.328702>.
6. van Eijkelenborg, M. A., Argyros, A., & Leon-Saval, S. G. (2008). Polycarbonate hollow-core microstructured optical fiber. *Optics Letters*, 33(21), 2446-2448. <http://dx.doi.org/10.1364/OL.33.002446>. PMID:18978882.
7. Cordeiro, C. M. B., Ng, A. K. L., & Ebendorff-Heidepriem, H. (2020). Ultra-simplified single-step fabrication of microstructured optical fiber. *Scientific Reports*, 10(1), 9678. <http://dx.doi.org/10.1038/s41598-020-66632-3>. PMID:32541807.
8. Faiz, F., Baxter, G., Collins, S., Sidirolou, F., & Cran, M. (2020). Polyvinylidene fluoride coated optical fibre for detecting perfluorinated chemicals. *Sensors and Actuators. B, Chemical*, 312, 128006. <http://dx.doi.org/10.1016/j.snb.2020.128006>.
9. Koike, Y., & Ishigure, T. (2006). High-bandwidth plastic optical fiber for fiber to the display. *Journal of Lightwave Technology*, 24(12), 4541-4553. <http://dx.doi.org/10.1109/JLT.2006.885775>.
10. Ferreira, R. A. S., André, P. S., & Carlos, L. D. (2010). Organic-inorganic hybrid materials towards passive and active architectures for the next generation of optical networks. *Optical Materials*, 32(11), 1397-1409. <http://dx.doi.org/10.1016/j.optmat.2010.06.019>.
11. Benabid, F., Knight, J. C., Antonopoulos, G., & Russell, P. S. J. (2002). Stimulated Raman scattering in hydrogen-filled hollow-core photonic crystal fiber. *Science*, 298(5592), 399-402. <http://dx.doi.org/10.1126/science.1076408>. PMID:12376698.
12. Sharma, D. K., Sharma, A., & Tripathi, S. M. (2018). Thermo-optic characteristics of hybrid polymer/silica microstructured optical fiber: an analytical approach. *Optical Materials*, 78, 508-520. <http://dx.doi.org/10.1016/j.optmat.2018.02.037>.
13. Li, C.-P., Tenent, R. C., & Wolden, C. A. (2020). Optical and mechanical properties of nanocomposite films based on Polymethyl Methacrylate (PMMA) and fumed silica nanoparticles. *Polymer Engineering and Science*, 60(3), 553-557. <http://dx.doi.org/10.1002/pen.25312>.
14. Anandhan, S., & Bandyopadhyay, S. (2011). *Polymer nanocomposites: from synthesis to applications*. In J. Cuppoletti (Ed.), *Nanocomposites and polymers with analytical methods* (pp. 1-28). London: IntechOpen. <http://dx.doi.org/10.5772/17039>.
15. Zhang, Y., & Luo, Y. (2021). Naturally derived nanomaterials for multidisciplinary applications and beyond. *ES Food & Agroforestry*, 4, 1-2. <http://dx.doi.org/10.30919/esfaf484>.
16. Islam, M. J., Rahman, M. J., & Mieno, T. (2020). Safely functionalized carbon nanotube-coated jute fibers for advanced technology. *Advanced Composites and Hybrid Materials*, 3(3), 285-293. <http://dx.doi.org/10.1007/s42114-020-00160-6>.
17. Lewicki, J. P., Rodriguez, J. N., Zhu, C., Worsley, M. A., Wu, A. S., Kanarska, Y., Horn, J. D., Duoss, E. B., Ortega, J. M., Elmer, W., Hensleigh, R., Fellini, R. A., & King, M. J. (2017). 3D-printing of meso-structurally ordered carbon fiber/polymer composites with unprecedented orthotropic physical properties. *Scientific Reports*, 7(1), 43401. <http://dx.doi.org/10.1038/srep43401>. PMID:28262669.
18. Qin, C., Gong, H., Sun, C., & Wu, X. (2021). Optical properties of a core/shell/shell shape metal-insulator-metal composite nanoparticle for solar energy absorption. *Engineered Science*, 17, 224-230. <http://dx.doi.org/10.30919/es8e509>.
19. Xue, J., & Luo, Y. (2021). Sustainable food and agriculture system: a nanotechnology perspective. *ES Food and Agroforestry*, 5, 1-3. <http://dx.doi.org/10.30919/esfaf538>.
20. Silva, E. A., Ribeiro, L. A., Nascimento, M. C. B. C., & Ito, E. N. (2014). Rheological and mechanical characterization of Poly (methyl methacrylate)/silica (PMMA/SiO₂) composites. *Materials Research*, 17(4), 926-932. <http://dx.doi.org/10.1590/S1516-14392014005000114>.
21. Pötschke, P., Fornes, T. D., & Paul, D. R. (2002). Rheological behavior of multiwalled carbon nanotube/polycarbonate composites. *Polymer*, 43(11), 3247-3255. [http://dx.doi.org/10.1016/S0032-3861\(02\)00151-9](http://dx.doi.org/10.1016/S0032-3861(02)00151-9).
22. Sun, X., Lasecki, J., Zeng, D., Gan, Y., Su, X., & Tao, J. (2015). Measurement and quantitative analysis of fiber orientation distribution in long fiber reinforced part by injection molding. *Polymer Testing*, 42, 168-174. <http://dx.doi.org/10.1016/j.polymertesting.2015.01.016>.
23. Prado, B. R., & Bartoli, J. R. (2018). Synthesis and characterization of PMMA and organic modified montmorillonites nanocomposites via in situ polymerization assisted by sonication. *Applied Clay Science*, 160, 132-143. <http://dx.doi.org/10.1016/j.clay.2018.02.035>.
24. Bressanin, J. M., Assis, V. A. Jr., & Bartoli, J. R. (2018). Electrically conductive nanocomposites of PMMA and carbon nanotubes prepared by in situ polymerization under probe sonication. *Chemical Papers*, 72(7), 1799-1810. <http://dx.doi.org/10.1007/s11696-018-0443-5>.
25. Chen, J., Zhu, Y., Guo, Z., & Nasibulin, A. G. (2020). Recent progress on thermo-electrical properties of conductive polymer composites and their application in temperature sensors. *Engineered Science*, 12, 13-22. <http://dx.doi.org/10.30919/es8d1129>.
26. Gu, H., Gao, C., Zhou, X., Du, A., Naik, N., & Guo, Z. (2021). Nanocellulose nanocomposite aerogel towards efficient oil and organic solvent adsorption. *Advanced Composites and Hybrid Materials*, 4(3), 459-468. <http://dx.doi.org/10.1007/s42114-021-00289-y>.
27. Yu, Z., Yan, Z., Zhang, F., Wang, J., Shao, Q., Murugadoss, V., Alhadhrami, A., Mersal, G. A. M., Ibrahim, M. M., El-Bahy, Z. M., Li, Y., Huang, M., & Guo, Z. (2022). Waterborne acrylic resin co-modified by itaconic acid and γ -methacryloxypropyl triisopropoxidesilane for improved mechanical properties, thermal stability, and corrosion resistance. *Progress in Organic Coatings*, 168, 106875. <http://dx.doi.org/10.1016/j.porgcoat.2022.106875>.
28. Chang, X., Chen, L., Chen, J., Zhu, Y., & Guo, Z. (2021). Advances in transparent and stretchable strain sensors. *Advanced Composites and Hybrid Materials*, 4(3), 435-450. <http://dx.doi.org/10.1007/s42114-021-00292-3>.
29. Münstedt, H., Köppl, T., & Triebel, C. (2010). Viscous and elastic properties of poly(methyl methacrylate) melts filled with silica nanoparticles. *Polymer*, 51(1), 185-191. <http://dx.doi.org/10.1016/j.polymer.2009.11.049>.
30. Triebel, C., & Münstedt, H. (2011). Temperature dependence of rheological properties of poly(methyl methacrylate) filled with silica nanoparticles. *Polymer*, 52(7), 1596-1602. <http://dx.doi.org/10.1016/j.polymer.2011.02.014>.
31. Zhang, Q., Huang, W.-X., & Zhong, G.-J. (2017). Towards transparent PMMA/SiO₂ nanocomposites with promising scratch-resistance by manipulation of SiO₂ aggregation followed by in situ polymerization. *Journal of Applied Polymer Science*, 134(12), 44612. <http://dx.doi.org/10.1002/app.44612>.
32. Mallakpour, S., & Naghdi, M. (2018). Polymer/SiO₂ nanocomposites: production and applications. *Progress in Materials Science*, 97, 409-447. <http://dx.doi.org/10.1016/j.pmatsci.2018.04.002>.
33. Jancar, J., & Recman, L. (2010). Particle size dependence of the elastic modulus of particulate filled PMMA near its

- T. *Polymer*, 51(17), 3826-3828. <http://dx.doi.org/10.1016/j.polymer.2010.06.041>.
34. Hu, F., Li, G., Zou, P., Hu, J., Chen, S., Liu, Q., Zhang, J., Jiang, F., Wang, S., & Chi, N. (2020). *20.09-Gbit/s underwater WDM-VLC transmission based on a single Si/GaAs-substrate multichromatic LED array chip*. In *Optical Fiber Communication Conference (OFC)* (pp. M31.4). Washington, D.C.: Optica Publishing Group. <http://dx.doi.org/10.1364/OFC.2020.M31.4>.
 35. Kachere, A. R., Kakade, P. M., Kanwade, A. R., Dani, P., Mandlik, N. T., Rondiya, S. R., Dzade, N. Y., Jadkar, S. R., & Bhosale, S. V. (2022). Zinc oxide graphene oxide nanocomposites: synthesis, characterization and their optical properties. *ES Materials & Manufacturing*, 16, 19-29.
 36. Wang, C., Wen, Y., Sun, J., & Zhou, J. (2022). Recent progress on optical frequency conversion in nonlinear metasurfaces and nanophotonics. *ES Materials & Manufacturing*, 17, 1-13. <http://dx.doi.org/10.30919/esmm5f655>.
 37. Zou, D. Q., & Yoshida, H. (2010). Size effect of silica nanoparticles on thermal decomposition of PMMA. *Journal of Thermal Analysis and Calorimetry*, 99(1), 21-26. <http://dx.doi.org/10.1007/s10973-009-0531-4>.
 38. Abramoff, B., & Covino, J. (1992). Transmittance and mechanical properties of PMMA-fumed silica composites. *Journal of Applied Polymer Science*, 46(10), 1785-1791. <http://dx.doi.org/10.1002/app.1992.070461009>.
 39. Taurozzi, J. S., Hackley, V. A., & Wiesner, M. R. (2011). Ultrasonic dispersion of nanoparticles for environmental, health and safety assessment – issues and recommendations. *Nanotoxicology*, 5(4), 711-729. <http://dx.doi.org/10.3109/17435390.2010.528846>. PMID:21073401.
 40. Price, G. J., Norris, D. J., & West, P. J. (1992). Polymerization of methyl methacrylate initiated by ultrasound. *Macromolecules*, 25(24), 6447-6454. <http://dx.doi.org/10.1021/ma00050a010>.
 41. Price, G. J. (2003). Recent developments in sonochemical polymerization. *Ultrasonics Sonochemistry*, 10(4-5), 277-283. [http://dx.doi.org/10.1016/S1350-4177\(02\)00156-6](http://dx.doi.org/10.1016/S1350-4177(02)00156-6). PMID:12818394.
 42. Kaino, T. (1985). Absorption losses of low loss plastic optical fibers. *Japanese Journal of Applied Physics*, 24(12R), 1661-1665. <http://dx.doi.org/10.1143/JJAP.24.1661>.
 43. Zhu, H., Wang, Y., Qu, M., Pan, Y., Zheng, G., Dai, K., Huang, M., Alhadhrami, A., Ibrahim, M. M., ElBahy, Z. M., Liu, C., Shen, C., & Liu, X. (2022). Electrospun poly(vinyl alcohol)/silica film for radiative cooling. *Advanced Composites and Hybrid Materials*, 5(3), 1966-1975. <http://dx.doi.org/10.1007/s42114-022-00529-9>.
 44. Si, Y., Li, J., Cui, B., Tang, D., Yang, L., Murugadoss, V., Maganti, S., Huang, M., & Guo, Z. (2022). Janus phenol-formaldehyde resin and periodic mesoporous organic silica nanoadsorbent for the removal of heavy metal ions and organic dyes from polluted water. *Advanced Composites and Hybrid Materials*, 5(2), 1180-1195. <http://dx.doi.org/10.1007/s42114-022-00446-x>.
 45. Bistac, S., & Schultz, J. (1997). Solvent retention in solution-cast films of PMMA: study by dielectric spectroscopy. *Progress in Organic Coatings*, 31(4), 347-350. [http://dx.doi.org/10.1016/S0300-9440\(97\)00093-3](http://dx.doi.org/10.1016/S0300-9440(97)00093-3).
 46. Padilha, G. S., Giaccon, V. M., & Bartoli, J. R. (2017). Effect of solvents on the morphology of PMMA films fabricated by spin-coating. *Polímeros: Ciência e Tecnologia*, 27(3), 195-200. <http://dx.doi.org/10.1590/0104-1428.12516>.
 47. Zhou, R.-J., & Burkhart, T. (2010). Optical properties of particle-filled polycarbonate, polystyrene, and poly(methyl methacrylate) composites. *Journal of Applied Polymer Science*, 115(3), 1866-1872. <http://dx.doi.org/10.1002/app.31331>.
 48. Yu, Y.-Y., Chen, C.-Y., & Chen, W.-C. (2003). Synthesis and characterization of organic-inorganic hybrid thin films from poly(acrylic) and monodispersed colloidal silica. *Polymer*, 44(3), 593-601. [http://dx.doi.org/10.1016/S0032-3861\(02\)00824-8](http://dx.doi.org/10.1016/S0032-3861(02)00824-8).
 49. Sunkara, H. B., Jethmalani, J. M., & Ford, W. T. (1994). Composite of colloidal crystals of silica in poly(methyl methacrylate). *Chemistry of Materials*, 6(4), 362-364. <http://dx.doi.org/10.1021/cm00040a006>.
 50. van de Hulst, H. C. (1958). Light scattering by small particles. *Quarterly Journal of the Royal Meteorological Society*, 84(360), 198-199.
 51. Zhao, J., Morgan, A. B., & Harris, J. D. (2005). Rheological characterization of polystyrene-clay nanocomposites to compare the degree of exfoliation and dispersion. *Polymer*, 46(20), 8641-8660. <http://dx.doi.org/10.1016/j.polymer.2005.04.038>.
 52. Schramm, G. (2006) *A practical approach to rheology and rheometry*. Karlsruhe: Thermo Electron (Karlsruhe) GmbH.
 53. Kotsilkova, R. (2007). *Thermoset nanocomposites for engineering applications*. Shawbury: Smithers Rapra Technology Limited.

Received: Jan. 27, 2022

Revised: Aug. 31, 2022

Accepted: Oct. 05, 2022

Supplementary Material

Supplementary material accompanies this paper.

Table S1. ANOVA table for UV-Vis transmittance values.

Table S2. ANOVA table for refractive indexes values.

Table S3. $G' = G''$, $\omega_{\text{crossover}}$ and λ values for the produced nanocomposites and pristine PMMA.

Figure S1. UV-Vis transmittance spectra of nanocomposites and pristine PMMA films.

Figure S2. Strain sweep analysis for rheological tests.

Figure S3. Rheological curves for the pristine PMMA sample.

Figure S4. Rheological curves for the sample: 4% A38-1.

Figure S5. Rheological curves for the sample: 4% A38-2.

Figure S6. Rheological curves for the sample: 4% A38-3.

Figure S7. Rheological curves for the sample: 2% A26.

Figure S8. Rheological curves for the sample: 2% A50.

Figure S9. Rheological curves for the sample: 6% A26.

Figure S10. Rheological curves for the sample: 6% A50.

Figure S11. Rheological curves for the sample: 4% C38-1.

Figure S12. Rheological curves for the sample: 4% C38-2.

Figure S13. Rheological curves for the sample: 4% C38-3.

Figure S14. Rheological curves for the sample: 2% C26.

Figure S15. Rheological curves for the sample: 2% C50.

Figure S16. Rheological curves for the sample: 6% C26.

Figure S17. Rheological curves for the sample: 6% C50.

This material is available as part of the online article from <https://doi.org/10.1590/0104-1428.20220009>